

Assessment Of Stress Concentration Factor At Hotspots On Non-uniform Corroded T-joints Under Axial Loading

Vu Dan Chinh*, Do Thanh Long, Hà Thi Thu Nguyễn, and Dinh Quang Cuong

Faculty of Coastal and Offshore Engineering, Hanoi University of Civil Engineering, 55 Giai phong str., Hai ba trung dist., Hanoi 100 000, Vietnam

* Corresponding author. E-mail: chinhvd@huce.edu.vn

Received: Apr. 10, 2023; Accepted: Oct. 12, 2023

After many years of operation, the corrosion phenomenon frequently appears on fixed steel offshore platforms. It changes the concentrated stress in joints, greatly increasing fatigue damage, and hastening structural collapse. This study examines the impact of corrosion at various regions along the chord of the compressive T-joint on the stress concentration factor (SCF) of the chord hotspots. Therefore, the region of influence is split into 15 shells. The impact ratio of the thickness in each shell on the SCF is estimated by using the numerical model in 54 scenarios of different corrosion. Also, a formula for calculating the equivalent thickness of a non-uniformly corroded chord is established using the regression approach. The condition that the SCF based on API employing equivalent thickness is comparable to the actual value of the hotspots on the corroded joint using gathered data is satisfied by this equation. Additionally, 4 scenarios for 2 numerical simulations of T-joints are used to validate the equation, together with surveying data from the White Tiger field. Additionally, using an experiment with compressive T-joints strengthened by doubler plates is used to compare the SCF. These outcomes all provide a good match for the new formula, which can reduce the SCF's computational time in similar conditions.

Keywords: non-uniform corrosion; tubular T-joint; axial loading; stress concentration factor (SCF); numerical models; equivalent thickness

© The Author(s). This is an open-access article distributed under the terms of the [Creative Commons Attribution License \(CC BY 4.0\)](https://creativecommons.org/licenses/by/4.0/), which permits unrestricted use, distribution, and reproduction in any medium, provided the original author and source are cited.

[http://dx.doi.org/10.6180/jase.202409_27\(9\).0008](http://dx.doi.org/10.6180/jase.202409_27(9).0008)

1. Introduction

Concentrated stress has a crucial role in the fatigue damage at hotspots and the service life of a fixed offshore platform. Due to a high exponential relation, a slight variation of the concentrated stress also causes significant changes in fatigue damage [1, 2]. For common structural members such as tubular joints, the concentrated stress at the hotspot is usually determined by multiplying the SCF with nominal stress. Therein, SCF is determined by empirical formulae, depending on the hotspot location, the type of joints, and the geometrical dimension of a chord and brace. The experimental equations proposed by Kwang, Efthymiou, or

Wordsworth/Smedley [3] are widely used and produce accurate results for simple joints like T, Y, K, X,... They were first introduced in standards [4–6]. The SCF at the hotspot has previously been studied for more complex joints, such as multi-planar tube joints or overlap joints [7–9]. Studies [10–13] presented the SCF on non-tubular and reinforced joints. They stated that a critical factor in determining the distribution of the concentrated stress was the geometric form of the chord/brace intersection. For tubular joints, we must strengthen the intersection to boost stiffness, such as by rings, adding doubler plates, or wrapping FRP to decrease SCF at the hotspot. In contrast, the SCF will significantly increase when these areas corrode.

There have been earlier studies on the strength and distribution of the tubular joint when taking the corrosion effect into account in recent years. The tubular stress distribution is generally impacted by a range of one to three times the chord outside diameter around the chord/brace intersection, according to earlier studies [14]. The thickness and area of corroded regions mainly cause stress fluctuation on joints. New hotspots with deep holes developing at local corroded positions were the main focus of research [15–17] regarding the SCF and fatigue strength of corroded joints.

However, based on survey data of the offshore steel platforms at the White Tiger field, Vietnam, non-uniform corrosion occurs popularly in both structural pipes and joints. Moreover, corrosion thicknesses on the same cross-section are significantly different. Typically, according to an investigation at the BK1 platform [18], for a chord thickness of 20.6 mm, after 25 years, the average difference in corrosion thickness on a cross-section is 3.48 mm, and the maximum difference is 6.5 mm. Similarly, at the MSP6 platform [19], the average corrosion thickness difference on a cross-section is 4.54 mm, and the maximum difference is 8 mm. The non-uniform corrosion typically manifests over a large area (Fig. 1 and Fig. 2) or near the junction of joints (Fig. 2). The geometric shape of joints will deteriorate as this corrosion region grows, resulting in an unexpected change in the stress distribution on the tubular joints. Therefore, more thorough investigations of the concentrated stress at the hotspot of non-corroded joints are required. When the corroded position and size changed for the same corroded thickness, Chinh et al. [2] found that the SCF significantly altered for the primary hotspots on the chord/brace intersection of the tubular joints. The previous empirical formulas were no longer appropriate in this case.



Fig. 1. Corroded platform BK-1 at White Tiger field (photo courtesy of VSP)



Fig. 2. A corroded tubular joint in platform MSP6 at White Tiger field (photo courtesy of VSP)

The influence of corrosion on the SCF at hotspots on the T-joint chord under compression in various zones is examined in this research. Then a new equation to compute the equivalent thickness of the chord is therefore proposed. The formula meets the requirement that the SCF at the crown and saddle of the corroded joint be equal to that at the same place of the chord with the corresponding thickness. The primary tool for conducting research is the numerical model ABAQUS. Following the use of these modelling findings and experimental formulae from API, a new equation of the equivalent thickness is developed. The proposed formula will be used to estimate the SCF in the aforementioned hotspots in accordance with actual corrosion data collected in the White Tiger field. Numerical simulations are frequently used to calculate concentrated stress at challenging locations in a structure. Compared to experimental laboratories, ABAQUS is shown to correspond well and produce accurate results [20–23]. In order to demonstrate the use and accuracy of the new equation, the physical results of SCFs at the saddle on the chord of the T-joint presented by Fung et al. [13] will be used to validate with API-based equivalent thickness.

2. Methods

2.1. SCF at saddle and crown on a chord based on API

In current standards, the SCF at the joint hotspots is determined through empirical formulae [4–6]. In the research of Chinh et al. [2], the authors compared the SCF values based on API and Lloyd's Register of tubular T-joints under axial loading. The comparison results are comparable, and the maximum difference is only about 6%. According to the API, the SCF at the crown and saddle on a chord of the T-joint under axial loading with fixed ends is calculated as follows (Table 1):

Table 1. SCF of Crown and Saddle based on API

Crown	Saddle
$SCF_{CC} = \gamma^{0.2} \tau \left(2.65 + 5(\beta - 0.65)^2 \right) (1)$ $+ \tau \beta (0.25\alpha - 3)$	$SCF_{SC} = \gamma \tau^{1.1} (1.11 - 3(\beta - 0.52)^2) (2)$

Where: $\alpha = \frac{2L}{D}$; $\beta = \frac{d}{D}$; $\gamma = \frac{D}{2T}$; $\tau = \frac{t}{T}$.

If considering corroded thickness has no impact on its outer diameter, the SCF at both the saddle and crown is inversely proportional to the chord thickness, with exponents of -1.2 and -2.1, respectively. The SCF is proportional to t with an approximate exponent of 1. Meanwhile, for an axial loading tubular, stress is inversely proportional to its chord area A since t is much smaller than d, so the brace area is a function of t in a relationship:

$$A = \pi(d - t) \cdot t = \pi (dt - t^2) \approx \pi dt \quad (3)$$

Therefore, when t changes, the increase of SCF will be approximately equal to the decrease of the nominal stress. It means when a brace is corroded, concentrated stress at hotspots is considered insignificant change. Therefore, the only effect of corrosion on hotspots of the chord is investigated in this paper.

2.2. Concentrated stress on a non-uniform corroded T-joint under axial loading

A T-joint is investigated as mentioned in Fig. 3. The outer diameter and thickness on the brace and the chord denote respectively d, t, and D, T. An axial compressive force P is put on the brace. The brace length l is selected short enough to stay the brace stable. The chord length L is long enough that does not impact stress distribution at the crossing of the brace and chord. Moreover, the ratio of L/D should be more than 6 [21]. The corroded area lies in the length of L_z. This area is divided into two zones to investigate the influence scale of corrosion on each area. Two ends of the restraint are fixed.

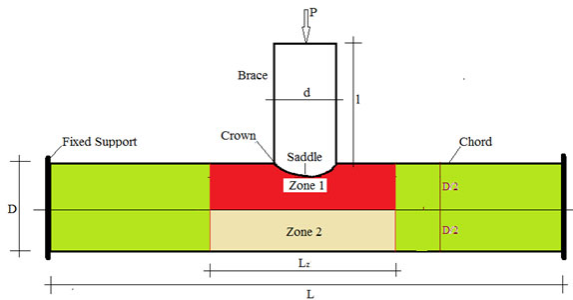


Fig. 3. A corroded T-joint sketch)

Three different forms of T-joints are taken into consideration when modelling in the SCF. Type 1 has a chord of DxT = 813x25mm, and a brace of dxt = 530x15mm. Type 2, chord DxT = 1020x30mm, brace dxt = 610x19mm. Type 3, chord DxT = 1270x30mm, brace dxt = 812x19mm. Joints are arranged by different corroded scenarios on chords. Material properties with E = 2x10⁵ MPa, ν = 0.3, Fy = 345 MPa are applied for all joints. P = 300 kN is putting in all braces. Since this research mainly focuses on the linear elastic stage, force P has not any influence on the SCF values. One more assumption

is the influence of axial force on pipe strength is insignificantly considered in this calculation.

Abaqus is used to simulate corroded joints [24]. Tubular joints are simulated by shell elements to reduce computational time and make a rapid change in thickness. The impact of weld geometry is not taken into account in the API formulae. The welding is therefore neglected in the numerical models. For fixed supports, reference points RP2 and RP3 are established at the chord's two ends, and for the axial load, reference point RP1 is designated at the top of the brace (Fig. 5). The work of the relevant sections is represented by the reference points. Tubular joints are divided by shell elements with four nodes S4R. Element dimension is chosen to assure the concentrated stress at hotspots is convergent. The comparison of SCF on various grid sizes has been examined in some studies [7, 8, 25]. In the paper, the SCF of hotspots on the chord of the different types above of non-corroding pipes—corresponding to grid sizes of 3 cm, 2 cm, and 1 cm—will be examined. The numerical results given in Fig. 4 demonstrate that the results start to converge in a 2 cm grid and that the highest deviation from the API standard is approximately 4%. Therefore, in the next scenarios of corrosion studies, the model adopts the grid size of 2 cm (Fig. 5).

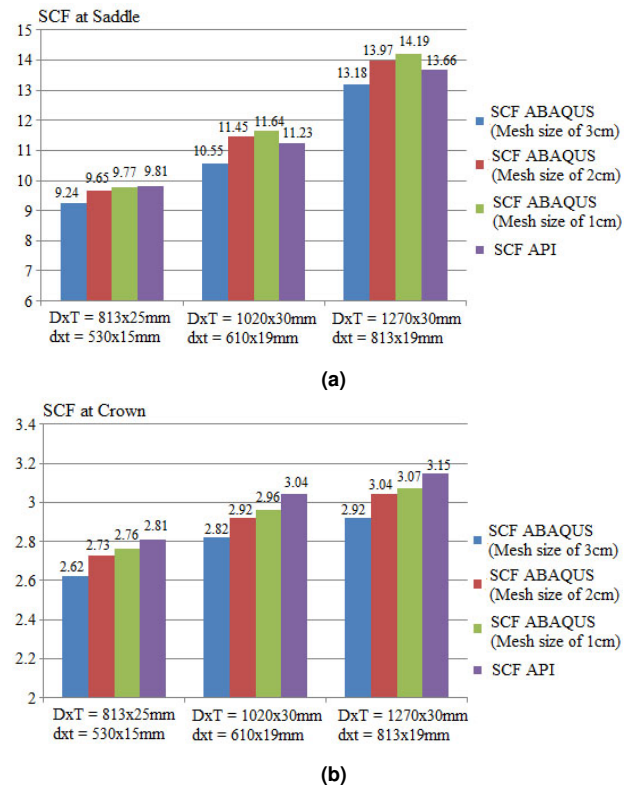


Fig. 4. SCF at hotspots in relation with different element sizes

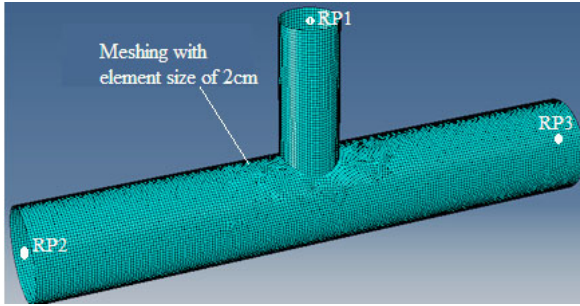


Fig. 5. Element grid of tubular joint Type 1

The element grids in the corroded zone are moved into modified coordinates that match the corroded thickness (Fig. 6). The Eq. (4) satisfy the new coordinate components x_c, y_c at any point on the chord with a corrosion thickness of ΔT [2].

$$x_c = \frac{D}{2} - \frac{\Delta T}{2} \cdot x; \quad y_c = \frac{D}{2} - \frac{\Delta T}{2} \cdot y \quad (4)$$

Where x and y are the pre-corrosion coordinates for that point.

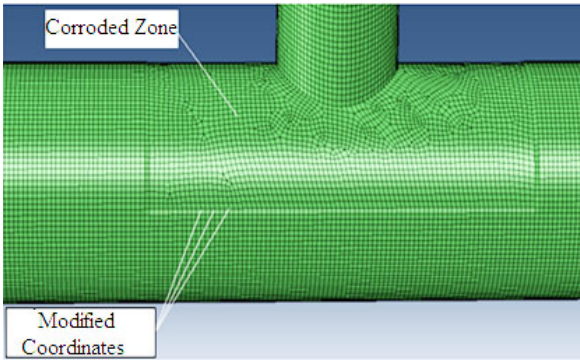


Fig. 6. Corroded area on a joint in Abaqus

2.3. Limitation of the corroded zone

Based on Mohamed et al. [24], regarding ultimate strength in corroded joints in physical models, a chord thickness in corroded area L_z takes approximately $3D$. In the research of Lesani et al. [22], the length of strengthened chords influences joint strength ($L_z = 2 \times 6\sqrt{DT}$). When the D/T ratio is smaller than 60, the minimum value of L_z is roughly $1.5D$. In this research, based on numerical analysis of T-joints in a uniform corroded chord, when L_z is greater than $2D+d$, the SCF at the saddle and crown of the chord can vary less than 8% in the same corroded thickness. Results are given in Table 2.

Based on the results from Table 3, the influence of zone 2 on SCF in the saddle and crown is relatively small. When all tubular thicknesses in zone 2 decrease by more than 35%, the SCF increases smaller than 6%. Therefore, the corrosion effects of this zone can be ignored, the research focuses mainly on zone 1, including from the center elevation to the top of the chord.

2.4. Non-uniform corroded scenarios

For existing platforms in Vietnam, corroded measurement is based on 4 points in each tubular section, at directions 0 h, 3 h, 6 h,

and 9 h as mentioned in Fig. 7. To match the survey data, this paper assumes each section is divided into four parts relying on inclined angles (see section A-A in Fig. 7), corroded thickness is considered a constant in each part. Based on the previous section, the interested corrosion area is the upper half of the chord in a length of $L_z=2D+d$. This area is divided into 5 segments including 15 shells with sequences from 1 to 15 in Fig. 7. Corroded thickness stays constant in each shell. This condition satisfies only when the width of shell 8 is more than the brace diameter. Corroded scenarios are chosen based on the change in thickness of one or more shells to investigate the effect of each corroded zone on the variation of the concentrated stress in the hotspots. Consequently, we establish a new formula to determine equivalent thickness in case the SCF at hotspots on a tubular joint is equal to that on a non-uniform corroded joint based on the actual survey data.

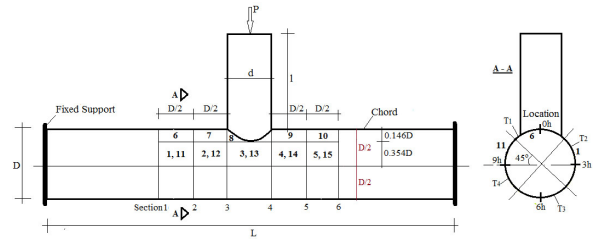


Fig. 7. Modelling of a non-uniform corroded tubular joint

To assure the application of API-based formulae, in this paper, the tubular and shell thicknesses in the numerical program are selected as follows. Firstly, the minimum thickness of the chord is greater than that of the brace plus 6 mm to fit with the design and survey data of platforms in the White Tiger field. It assures the chord thickness is still more than that in the brace after exploiting an entire structural design’s lifetime. Secondly, the minimum thickness in the corroded shell is taken approximately the brace thickness value.

To limit the number of trial tests in the regression approach, corroded scenarios are selected according to the following steps.

1. Each shell is assigned a minimum thickness, where the thickness of the remaining shells stays unchanged compared with the original value. These scenarios are used to estimate the influence of each corroded shell on the SCF at the hotspots. Then, the most influential shell can be determined.

2. Keep the thickness of the most influential shell constant. One of the remaining shells is assigned a minimum thickness while the others still stay the same. Consequently, we can find the influence of the following shell.

The above step is repeated to determine the sequences of the third shell to the last one.

Note that the shell and hotspot are symmetric through the brace axis, and the asymmetric shells are assigned the same thickness in scenarios. In actual projects, the most dangerous hotspot has higher concentrated stress in shells with different thicknesses.

Based on this discipline, scenarios are applied for three types of joints. Joint type 1: Chord $D \times t = 813 \times 25$ mm, brace $d \times t = 530 \times 15$ mm, $L = 5$ m, $l = 2$ m. Joint type 2: Chord $D \times t = 1020 \times 30$ mm, brace $d \times t = 610 \times 19$ mm, $L = 6.5$ m, $l = 2$ m. Joint type 3: Chord $D \times t = 1270 \times 30$ mm, brace $d \times t = 812 \times 19$ mm, $L = 8$ m, $l = 2$ m. Thicknesses of corroded shells are given in Table 4. 54 tests have been simulated by Abaqus. Results are given in the following section.

Table 2. Limitation of corroded length

Database id.	DxT [mm]	dxt [mm]	L [m]	1 [m]	Tz1=Tz2 [mm]	Lz [m]	SCF saddle	SCF crown
TH-01	813x25	530x15	5	2	16	1.4	20.14	4.60
TH-02						2.2	23.65	4.67
TH-03						5	24.90	4.74
TH-04	1020x30	610x19	6.5	2	20	1.9	22.45	4.21
TH-05						2.7	24.80	4.65
TH-06						6.5	26.21	4.94
TH-07	1270x30	812x19	8	2	20	2	26.13	4.93
TH-08						3.4	29.59	5.21
TH-09						8	31.50	5.54

Table 3. Effect of corrosion in zone 2

Database id.	DxT [mm]	dxt [mm]	L [m]	1 [m]	Tz1=Tz2 [mm]	Lz [m]	SCF saddle	SCF crown
TH-10	813x25	530x15	5	2	2.2	16	10.85	3.00
TH-11						20	10.61	2.95
TH-12						25	10.29	2.87
TH-13	1020x30	610x19	6.5	2	2.7	20	12.19	3.07
TH-14						25	11.90	2.98
TH-15						30	11.78	2.90
TH-16	1270x30	812x19	8	2	3.4	20	14.90	3.21
TH-17						25	14.52	3.10
TH-18						30	14.31	3.04

3. Results discussion

3.1. Stress concentration factors (SCFs) at saddle and crown points

SCFs can be determined based on the following basic equations:

$$SCF_{SC} = \frac{\sigma_{SC}}{\sigma_n}; \quad SCF_{CC} = \frac{\sigma_{CC}}{\sigma_n} \quad (5)$$

Where SCF_{SC} and SCF_{CC} are the stress concentration factors at a saddle point and a crown point, respectively; σ_{SC} and σ_{CC} are the concentration stresses at related hotspots, respectively, estimated based on a numerical model. The numerical stress value at a hotspot is determined based on ABS [26], mentioned in [2]. σ_n denotes the nominal stress on a compressive brace.

Analysis results of the concentration stress are summarized in Table 5. Fig. 8 shows a typical concentrated stress distribution at a tubular joint.

The above results indicate the effect of each corroded zone on the SCF at the saddle and the crown. The corrosion at shell T8 causes the most significant change in SCF at the hotspot in the same thickness. Next is the change of shells T3 and T13. After that are the effects of shells T2, T4, T12, and T14. Finally, the influences of T1, T5, T11, T15 and T6, T7, T9, T10 are approximately equal and relatively small. For instance, in the cases TC01 to TC09, TC19 to TC27 and TC37 to TC45, it is shown that when the thickness T8 decreases, the SCF at the saddle on the chord rises from 43% to 49% in comparison to that of the pre-corrosion. The SCF at the saddle rises from 61% to 79% when the T8, T3, and T13 thicknesses decrease. The SCF only increases by about 10% when the remaining

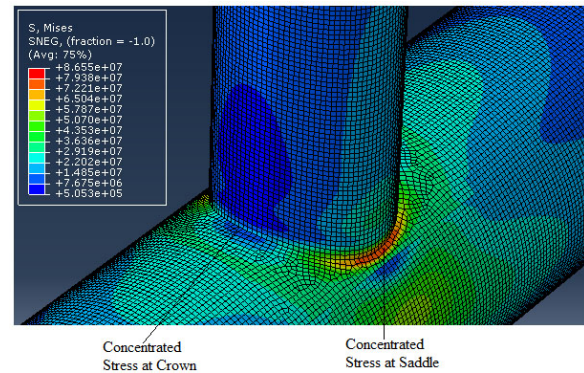


Fig. 8. Concentrated stress distribution on a typical tubular T-joint

shells decreases.

In addition, the influence of shells on SCF at the saddle and crown is quite similar in the above order. It is convenient to create a new equation for equivalent tubular thickness to estimate SCF for both hotspots. Based on the above results, a new formula will be proposed in the next section.

3.2. A new equation of SCF at hotspots

In this paper, three hypotheses will be made. Firstly, shells at the same position have a similar influence on SCF at the above hotspots. Then, different thicknesses at the symmetrical position

Table 4. Shell thickness of corroded chord of T-joints

		TC 01	TC 02	TC 03	TC 04	TC 05	TC 06	TC 07	TC 08	TC 09	TC 10	TC 11	TC 12	TC 13	TC 14	TC 15	TC 16	TC 17	TC 18
T1, T11		25	25	25	16	16	25	25	25	25	25	25	25	19	19	25	25	25	25
T2, T12		25	25	25	25	25	16	16	25	25	25	25	25	25	25	19	19	25	25
T3, T13		25	16	16	25	25	25	25	25	25	19	19	25	25	25	25	25	25	25
T4, T14		25	25	25	25	25	16	16	25	25	25	25	25	25	19	19	25	25	25
T5, T15		25	25	25	16	16	25	25	25	25	25	25	19	19	25	25	25	25	25
T6, T10		25	25	25	25	25	25	16	16	25	25	25	25	25	25	25	25	19	19
T7, T9		25	25	25	25	25	25	16	16	25	25	25	25	25	25	25	25	19	19
T8		16	16	25	16	25	16	25	25	16	19	19	25	19	25	19	25	25	19
		TC 19	TC 20	TC 21	TC 22	TC 23	TC 24	TC 25	TC 26	TC 27	TC 28	TC 29	TC 30	TC 31	TC 32	TC 33	TC 34	TC 35	TC 36
T1, T11		30	30	30	20	20	30	30	30	30	30	30	30	25	25	30	30	30	30
T2, T12		30	30	30	30	30	20	20	30	30	30	30	30	30	30	25	25	30	30
T3, T13		30	20	20	30	30	30	30	30	30	30	25	25	30	30	30	30	30	30
T4, T14		30	30	30	30	30	20	20	30	30	30	30	30	30	30	25	25	30	30
T5, T15		30	30	30	20	20	30	30	30	30	30	30	30	25	25	30	30	30	30
T6, T10		30	30	30	30	30	30	30	20	20	30	30	30	30	30	30	30	25	25
T7, T9		30	30	30	30	30	30	30	20	20	30	30	30	30	30	30	30	25	25
T8	20	20	30	20	30	20	30	30	20	25	25	30	25	30	25	30	30	25	
		TC 37	TC 38	TC 39	TC 40	TC 41	TC 42	TC 43	TC 44	TC 45	TC 46	TC 47	TC 48	TC 49	TC 50	TC 51	TC 52	TC 53	TC 54
T1, T11		30	30	30	20	20	30	30	30	30	30	30	30	25	25	30	30	30	30
T2, T12		30	30	30	30	30	20	20	30	30	30	30	30	30	30	25	25	30	30
T3, T13		30	20	20	30	30	30	30	30	30	30	25	25	30	30	30	30	30	30
T4, T14		30	30	30	30	30	20	20	30	30	30	30	30	30	30	25	25	30	30
T5, T15		30	30	30	20	20	30	30	30	30	30	30	30	25	25	30	30	30	30
T6, T10		30	30	30	30	30	30	30	20	20	30	30	30	30	30	30	30	25	25
T7, T9		30	30	30	30	30	30	30	20	20	30	30	30	30	30	30	30	25	25
T8	20	20	30	20	30	20	30	30	20	25	25	30	25	30	25	30	30	25	

Note: For type 1: TC01 to TC18, type 2: TC19 to TC36, and type 3: TC37 to TC54. Dimension used is mm for all shells.

are represented by average thickness. Finally, the equivalent formula will be applied unitedly to estimate the equivalent SCF for both the saddle and the crown. Therefore, the basic equation of an equivalent chord thickness can be expressed:

$$T_{eq} = a_1 T_8 + a_2 \frac{T_3 + T_{13}}{2} + a_3 \frac{T_2 + T_{12}}{2} + a_4 \frac{T_4 + T_{14}}{2} + a_5 \frac{T_1 + T_{11}}{2} + a_6 \frac{T_5 + T_{15}}{2} + a_7 \frac{T_6 + T_{10}}{2} + a_8 \frac{T_7 + T_9}{2} \tag{6}$$

on condition that: $\sum_{i=1}^8 a_i = 1$.

Based on the result of 54 test cases mentioned in Table 5, an approximation approach is performed in each case in order to satisfy:

$$\begin{aligned} SCF_S(T_{eq}) &\approx SCF_{SC} \\ SCF_C(T_{eq}) &\approx SCF_{CC} \end{aligned} \tag{7}$$

Where $SCF_S(T_{eq})$ and $SCF_C(T_{eq})$ denote the stress concentration factor at the saddle and the crown on a chord of a tubular T-joint using Eq. (1) and Eq. (2).

The results as: $a_1 = 0.51; a_2 = 0.17; a_3 = a_4 = 0.08; a_5 = a_6 = a_7 = a_8 = 0.04$. Eq. (6) can be rewritten as (8). The SCF results derived by API with equivalent chord thickness estimated by Eq. (8) are summarized in Table 6.

$$\begin{aligned} T_{eq} = &0.51T_8 + 0.17 \frac{T_3 + T_{13}}{2} + 0.08 \frac{T_2 + T_{12}}{2} + 0.08 \frac{T_4 + T_{14}}{2} \\ &+ 0.04 \frac{T_1 + T_{11}}{2} + 0.04 \frac{T_5 + T_{15}}{2} + 0.04 \frac{T_6 + T_{10}}{2} + 0.04 \frac{T_7 + T_9}{2} \end{aligned} \tag{8}$$

The coefficient of determination R^2 can be estimated based on the regression approach:

$$R^2 = 1 - \frac{S_e}{S_T} \tag{9}$$

where

$$\begin{aligned} S_e &= \sum_{k=1}^{54} (SCF_k - SCF_k(T_{eq}))^2 \\ S_T &= \sum_{k=1}^{54} (SCF_k - \text{Mean}(SCF))^2 \end{aligned} \tag{10}$$

According to Table 5 and Table 6, the coefficient of determination at the saddle $R^2 = 0.98$, and the crown $R^2 = 0.97$. Therefore, the Eq. (8) is well matched to estimate the SCF in API for the equivalent thickness at both the saddle and crown points of a corroded joint.

Table 5. Results of SCF at the hotspots on a non-uniform corroded T-joint in the numerical model

Case id	TC01	TC02	TC03	TC04	TC05	TC06	TC07	TC08	TC09	TC10	TC 11
σ_n [MPa]	12.37	12.37	12.37	12.37	12.37	12.37	12.37	12.37	12.37	12.37	12.37
σ_{SC} [MPa]	174.6	214.28	127.85	189.85	125.7	196.67	130.47	131.96	188.74	153.31	169.53
σ_{CC} [MPa]	47.87	52.55	35.87	48	33.58	49.81	35.54	34.16	50.61	42.85	45.52
SCF_{SC}	14.11	17.32	10.34	15.35	10.76	15.9	10.55	10.67	15.26	12.4	13.71
SCF_{CC}	3.87	4.25	2.9	3.88	2.72	4.03	2.87	2.76	4.09	3.46	3.68
Case id	TC12	TC13	TC14	TC15	TC16	TC17	TC18	TC19	TC20	TC21	TC22
σ_n [MPa]	12.37	12.37	12.37	12.37	12.37	12.37	12.37	8.51	8.51	8.51	8.51
σ_{SC} [MPa]	127.78	158.2	124.52	166.49	128.29	129.27	160.1	143.75	154.91	103.84	146
σ_{CC} [MPa]	34.9	42.8	33.44	43.95	34.67	33.66	44.46	35.26	37.87	26.21	34.95
SCF_{SC}	10.33	12.79	10.07	13.46	10.37	10.45	12.94	16.78	18.1	12.2	17.16
SCF_{CC}	2.82	3.46	2.7	3.55	2.8	2.72	3.6	4.14	4.45	3.08	4.11
Case id	TC23	TC24	TC25	TC26	TC27	TC28	TC29	TC30	TC31	TC32	TC33
σ_n [MPa]	8.51	8.51	8.51	8.51	8.51	8.51	8.51	8.51	8.51	8.51	8.51
σ_{SC} [MPa]	100.81	151.09	104.95	108.01	157.53	115.87	121.47	102.45	117.26	99.71	119.85
σ_{CC} [MPa]	25.36	36.91	25.96	25.57	35.24	29.41	30.53	25.99	29.17	25.06	30.03
SCF_{SC}	11.85	17.76	12.33	12.69	18.51	13.62	14.28	12.04	13.78	11.72	14.09
SCF_{CC}	2.98	4.34	3.05	3.01	4.14	3.46	3.59	3.05	3.43	2.95	3.53
Case id	TC34	TC35	TC36	TC37	TC38	TC39	TC40	TC41	TC42	TC43	TC44
σ_n [MPa]	8.51	8.51	8.51	6.33	6.33	6.33	6.33	6.33	6.33	6.33	6.33
σ_{SC} [MPa]	101.95	103.38	121.8	125.71	141.59	89.91	131.1	91.98	137.71	96.24	96.79
σ_{CC} [MPa]	25.92	25.24	28.63	27	29.51	19.79	27.21	19.63	28.75	19.99	19.54
SCF_{SC}	11.98	2.15	14.32	19.85	22.36	14.2	20.7	14.52	21.74	15.2	15.28
SCF_{CC}	3.05	2.97	3.37	4.26	4.36	3.13	4.3	3.1	4.54	3.16	3.09
Case id	TC45	TC46	TC47	TC48	TC49	TC50	TC51	TC52	TC53	TC54	-
σ_n [MPa]	6.33	6.33	6.33	6.33	6.33	6.33	6.33	6.33	6.33	6.33	-
σ_{SC} [MPa]	136.17	106.05	11.13	91.88	107.43	91.01	109.98	93.02	93.49	110.52	-
σ_{CC} [MPa]	28.41	22.9	23.71	19.55	22.74	18.93	23.41	19.3	18.77	22.89	-
SCF_{SC}	21.5	16.75	17.55	14.51	16.96	14.37	17.37	14.69	14.76	17.45	-
SCF_{CC}	4.49	3.62	3.74	3.09	3.59	2.99	3.7	3.05	2.96	3.62	-

Table 6. SCF result at hotspots on a T-joint based on API and the equivalent thickness

database id	TC01	TC02	TC03	TC04	TC05	TC06	TC07	TC08	TC09
SCF_{SC}	15.03	17.64	11.17	16.17	10.5	17.45	11.07	10.41	16.17
SCF_{CC}	3.58	3.92	3.02	3.73	2.92	3.9	3.01	2.9	3.73
database id	TC10	TC11	TC12	TC13	TC14	TC15	TC16	TC17	TC18
SCF_{SC}	12.95	14.28	10.68	13.46	10.23	14.14	10.68	10.23	13.46
SCF_{CC}	3.29	3.48	2.95	3.36	2.88	3.46	2.95	2.88	3.36
database id	TC19	TC20	TC21	TC22	TC23	TC24	TC25	TC26	TC27
SCF_{SC}	16.61	19.09	12.69	17.79	11.89	19.09	11.8	11.89	18.75
SCF_{CC}	3.8	4.12	3.26	3.95	3.14	4.12	3.13	3.14	4.08
database id	TC28	TC29	TC30	TC31	TC32	TC33	TC34	TC35	TC36
SCF_{SC}	13.58	14.46	11.89	13.9	11.55	14.34	11.89	11.55	13.9
SCF_{CC}	3.39	3.51	3.14	3.44	3.09	3.5	3.14	3.09	3.44
database id	TC37	TC38	TC39	TC40	TC41	TC42	TC43	TC44	TC45
SCF_{SC}	20.2	23.44	15.44	21.64	14.36	23.23	14.36	14.46	21.64
SCF_{CC}	3.94	4.29	3.38	4.1	3.24	4.26	3.24	3.26	4.1
database id	TC46	TC47	TC48	TC49	TC50	TC51	TC52	TC53	TC54
SCF_{SC}	16.53	17.59	14.46	17.04	14.05	17.45	14.46	14.05	17.07
SCF_{CC}	3.51	3.64	3.26	3.57	3.2	3.62	3.26	3.2	3.57

3.3. Verification of new formula

3.3.1. Application to the White Tiger field

Taking into account the two T-joints in the BK1 platform with listed data in Table 7. Material properties with $E = 2 \times 10^5 \text{MPa}$, $\nu =$

0.3 , $F_y = 345 \text{MPa}$ are applied for all joints. The restraint condition at two ends is fixed in all cases. The corrosion information gathered in the White Tiger field with 15 shells and listed in Table 8. Where, cases VC-01, VC-02 are applied for Joint 1 and cases VC-03, VC-04

Table 7. Joint model data

Joint ID	D (mm)	T (mm)	d (mm)	t (mm)	L (m)	P (kN)
Joint 1	812.8	20.62	530	12.6	5	300
Joint 2	610	16	325	11	4	100

are applied for Joint 2.

Corrosion simulation in ABAQUS and concentrated stress distribution on the tubular joints in scenarios are shown in Figs. 9 to 16. The comparison results of numerical models and based on API with equivalent chord thicknesses are exhibited in Table 10. The table shows that for various joint sizes and corrosion scenarios, the SCFs in the saddle and crown of the chord in API with using the proposed equivalent thickness are comparable to those in the numerical simulation for the surveying corrosion data. It confirms the equivalent thickness is satisfied and can be applied in complicated corroded joints.

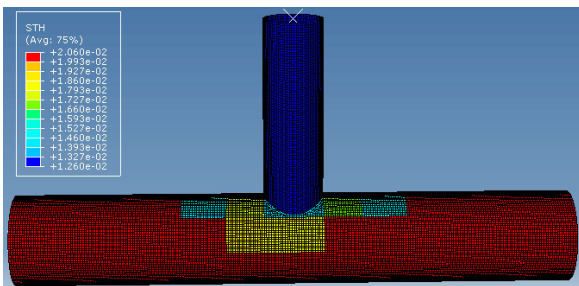


Fig. 9. Thickness distribution of corroded chord at a joint in surveying data – Case VC-01

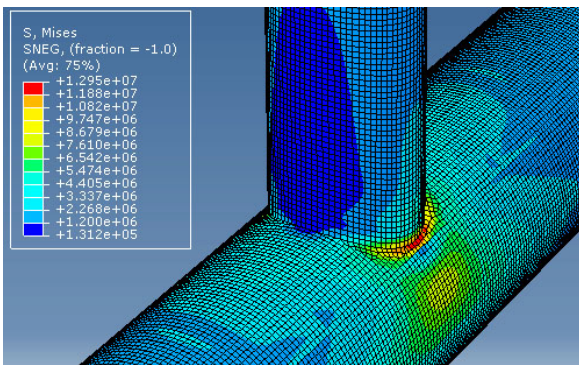


Fig. 10. Concentrated stress distribution on the saddle and crown – Case VC-01

3.3.2. Comparison with experimental results of compressive T-joints strengthened by doubler plates

There have not been any experiments that are relevant to this field of study so far. This section will present a validation of a study suggested by Fung et al. [13] regarding the concentrated stress of compressive T-joints strengthened by doubler plates in order to provide confirmation of the reliability of this work. The geometric

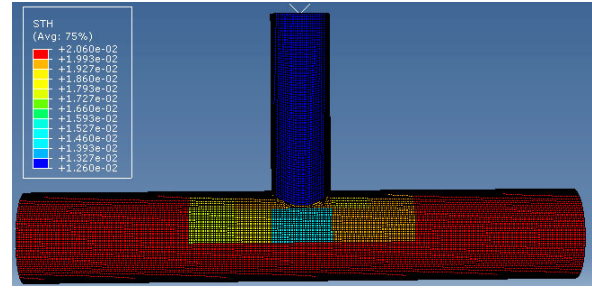


Fig. 11. Thickness distribution of corroded chord at a joint in surveying data – Case VC-02

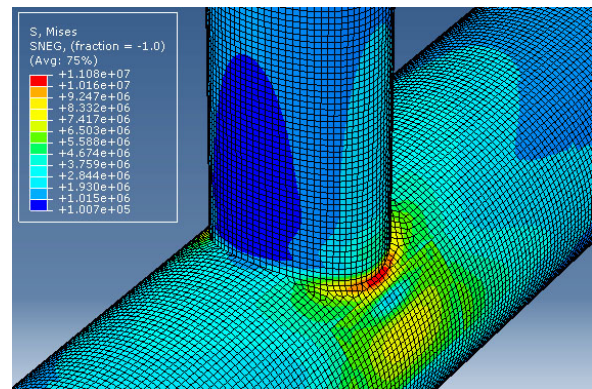


Fig. 12. Concentrated stress distribution on the saddle and crown – Case VC-02

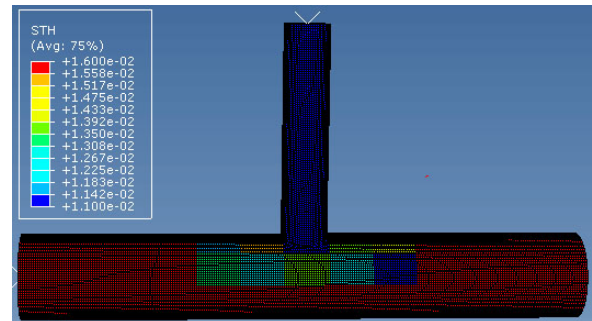


Fig. 13. Thickness distribution of corroded chord at a joint in surveying data – Case VC-03

information of joint is shown in Fig. 17. The experimental model used steel with Young’s modulus $E = 2 \times 10^5 \text{MPa}$, $\nu = 0.28$, $F_y = 345 \text{MPa}$. The compression force on the brace is $P = 49.86 \text{ kN}$ [13].

In 4 demonstrations, the SCF at the saddle will be compared in this section. A chord thickness of 9.5mm characterizes Case 1, a non-strengthened joint (Fig. 18). At the brace intersection zone in Case 2 (Fig. 19), the chord thickness increases by two times (19 mm). Case 3 is an experimental case in Fung et al. [13], the joint is reinforced by a plate that have the same thickness as the chord in Fig. 17 (9.5 mm). Case 4 is a 19mm chord-thick non-strengthened joint. The SCF is calculated in Cases 1 and 4 using API and numerical simulation. In Case 2, the SCF will be determined by the Abaqus model and API’s formula with equivalent thickness ob-

Table 8. Scenarios of shell thickness on corroded T-joints

Case VC-01	thickness [mm]	shell 1	shell 2	shell 3	shell 4	shell 5	shell 6	shell 7	shell 8
	thickness [mm]	shell 9	shell 10	shell 11	shell 12	shell 13	shell 14	shell 15	-
Case VC-02	thickness [mm]	shell 1	shell 2	shell 3	shell 4	shell 5	shell 6	shell 7	shell 8
	thickness [mm]	shell 9	shell 10	shell 11	shell 12	shell 13	shell 14	shell 15	-
Case VC-03	thickness [mm]	shell 1	shell 2	shell 3	shell 4	shell 5	shell 6	shell 7	shell 8
	thickness [mm]	shell 9	shell 10	shell 11	shell 12	shell 13	shell 14	shell 15	-
Case VC-04	thickness [mm]	shell 1	shell 2	shell 3	shell 4	shell 5	shell 6	shell 7	shell 8
	thickness [mm]	shell 9	shell 10	shell 11	shell 12	shell 13	shell 14	shell 15	-

Table 9. Comparative results of SCF

Case	Teq [mm]	SCF(Teq) at saddle in API	SCF(Teq) at crown in API	SCF max at saddle in ABAQUS	SCF max at crown in ABAQUS	% error SCF at saddle	% error SCF at crown
VC-01	16.7	18.89	3.82	18.34	3.89	3%	1.7
VC-02	19.3	13.94	3.21	13.57	3.09	2.7%	3.9%
VC-03	12.5	23.52	4.66	22.42	4.45	4.9%	4.7%
VC-04	13.6	19.70	4.22	19.24	4.26	2.4%	0.95%

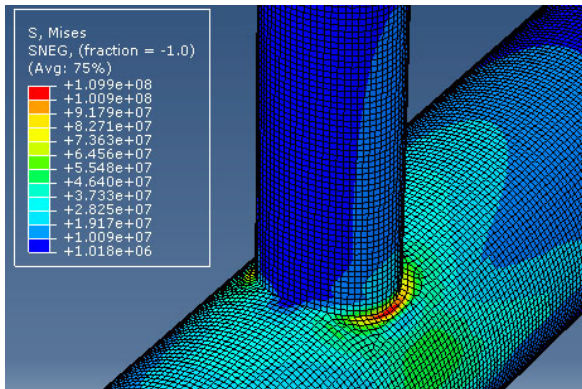


Fig. 14. Concentrated stress distribution on the saddle and crown – Case VC-03

tained by Eq. (8). Note that the chord section also changes in this situation because there is strengthening instead of corrosion at the chord-brace intersection. In Case 3, the SCF was acquired in a lab as part of their research. For the case of axial compression, the experimental result of hotspot strain at saddle point is $\approx 710 \times 10^{-6}$, so the hotspot stress is $2 \times 10^5 \times 710 \times 10^{-6} = 144$ MPa, then the SCF = $144/13.85 = 10.4$. Where 13.85 MPa is the nominal stress on the brace [13].

In Case 2, the average thickness of the i^{th} ($i = 1 \div 15$) shell can be calculated using Eq. (11) (Fig. 18). Whereas, $A_{9.5}$ A_{19} are the

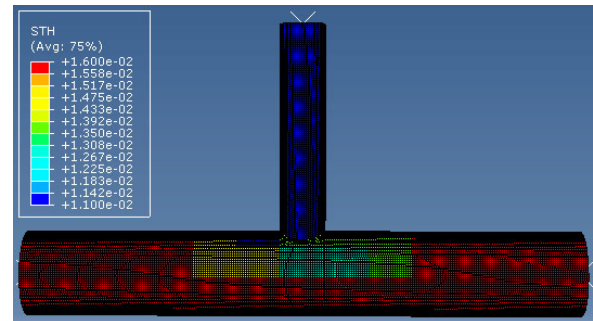


Fig. 15. Thickness distribution of corroded chord at a joint in surveying data – Case VC-04

areas of the corresponding shell thickness of 9.5 mm and 19 mm, respectively, and A_i is the area of the i^{th} shell.

$$T_i = \frac{A_{9.5}9.5 + A_{19}19}{A_i} \text{ (mm)} \quad (11)$$

Based on Fig. 20 and Eq. (11), $T_1 = T_5 = T_{11} = T_{15} = T_6 = T_{10} = 9.5\text{mm}$, $T_8 = 19\text{mm}$, $T_3 = T_{13} = 12.10\text{mm}$, $T_2 = T_{12} = T_4 = T_{14} = 11.20\text{mm}$, $T_7 = T_9 = 15.50\text{mm}$. Substituting those into Eq. (8), we have $T_{eq} = 15.30$ mm. The SCF results for cases are shown in Table 10.

According to API and ABAQUS, the SCFs in Cases 1 and Case 4 are comparable. Just over 2% of error is the maximum. It demon-

Table 10. SCF results at Saddle point

SCF Case 1 (API)	SCF Case 1 (ABAQUS)	SCF Case 2 (API with T_{eq})	SCF Case 2 (ABAQUS)	SCF Case 3	SCF Case 4 (API)	SCF Case 4 (ABAQUS)
18.16	18.5	6.96	7.08	10.40	4.24	4.22

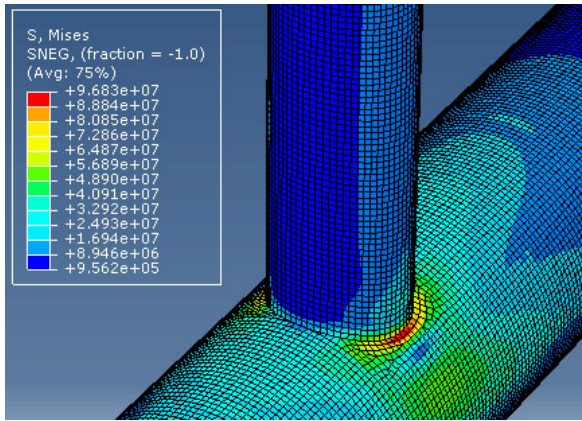


Fig. 16. Concentrated stress distribution on the saddle and crown – Case VC-04

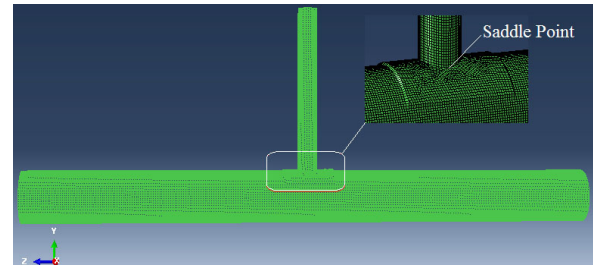


Fig. 19. Joint with a thickness strengthened by 2 times at the intersection zone – Case 2

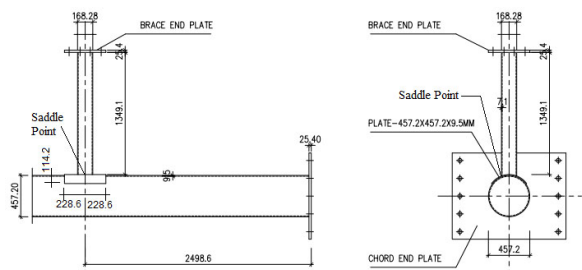


Fig. 17. An experimental sketch in Fung et al. [13]

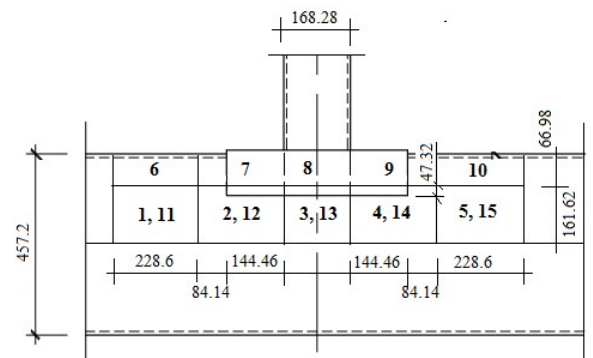


Fig. 20. Dimension of shells in joint model of Case 2

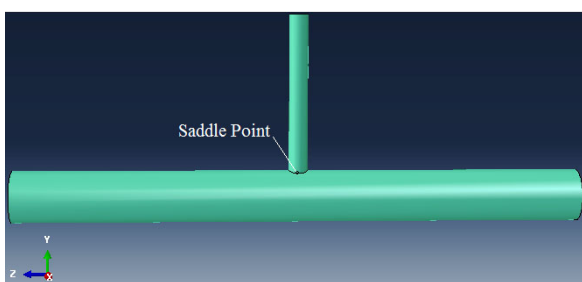


Fig. 18. Sketch of a non-strengthened joint – Cases 1 and 4

strates that the numerical model is accurate. The SCF value based on API with the equivalent thickness and the value in ABAQUS in Case 2 is comparable with a 1.7% error. Comparing Cases 2 and 3, the SCF in Case 2 is slightly lower than that in Case 3 experiment. It makes sense and is easily explained that Case 3 employs a removable cover and only utilizes welding to connect to the chord on the shell’s edge, making it more flexible than an intact shell of increasing thickness. In all of the cases, the SCF values are

reasonable. The aforementioned findings show that the suggested equation of the equivalent thickness in Eq. (8) for calculating the SCF is accurate and trustworthy.

4. Conclusions

It is known from the state-of-the-art that the chord thickness is a crucial factor in determining the concentrated stress at the chord/brace intersection. The stress will decrease as the thickness increases and vice versa. Therefore, the concentrated stress may change depending on the various non-uniform corrosion circumstances of the chord.

In this research, the effect of different chord corrosion zones on the variation of the SCF at the saddle and crown of a compressive T-joint is discussed. As a result, the most significant impact is caused by the corroded zone on the upper half of the chord and in a range of a length $2D+d$ surrounding the chord/brace intersection. Corrosion on the remaining tubular has an insignificant impact, varying by about 10%.

Also, the influence zone is divided into 15 shells in the study. The thickness is regarded as constant and affects the SCF value differently according to each shell. There, the shells directly beneath brace T8, T3, and T13 have the greatest impact. Shells at positions T2, T4, T12, and T14 are next. The remaining shells provide little

effect. This fits very nicely with earlier and related research. Moreover, this shell division is simple to use with data from the current Vietnam pipe corrosion surveying.

Last but not least, the study proposes a formula of the equivalent thickness on a non-uniform corroded chord in determining the SCF at the saddle and crown of T-joints in accordance with API. This formula is established based on the least squares regression method of 54 corrosion scenarios and 3 different tubular joints. The coefficient of determination $R^2 = 0.97$ indicates the fit of the approach. This equation is also validated on 2 different tubular joints and 4 non-uniform corrosion cases based on survey data in the White Tiger field. Moreover, a comparison between the SCFs based on API with the equivalent thickness, the numerical simulation and a previous experiment based on data of a T-joint strengthened by doubler plates is well-matched.

The limitation of corrosion in the tubular joint is that the equivalent thickness of the chord is greater than that in the brace. This requirement guarantees the application of the SCF equation at hotspots in the API standard.

References

- [1] N. D. Barltrop and A. J. Adams. *Dynamics of fixed marine structures*. 91. Butterworth-Heinemann, 2013.
- [2] V. D. Chinh et al., (2023) "Corrosion effect on stress concentration factor in tubular T-joints under axial loading" **Journal of Science and Technology in Civil Engineering (JSTCE)-HUCE** 17(3): 154–165.
- [3] L. Register, (1997) "Stress concentration factors for simple tubular joints, *Lloyds Register of Shipping—Offshore Division, Vols*":
- [4] A. RP2A-WSD, (2000) "Recommended practice for planning, designing and constructing fixed offshore platforms—working stress design—" **Twenty-2000**:
- [5] D. N. Veritas. *Fatigue design of offshore steel structures. Recommended Practice*. Tech. rep. DNV-RP-C203, 2011.
- [6] L. R. Rules. *Rules for the Classification of Offshore Units*. Tech. rep. Lloyd's Register Group Limited, 2022.
- [7] H. Ahmadi and A. Kouhi, (2020) "Stress concentration factors of multi-planar tubular XT-joints subjected to out-of-plane bending moments" **Applied Ocean Research** 96: 102058. DOI: [10.1016/j.apor.2020.102058](https://doi.org/10.1016/j.apor.2020.102058).
- [8] E. Zavvar, K. Hectors, and W. De Waele, (2021) "Stress concentration factors of multi-planar tubular KT-joints subjected to in-plane bending moments" **Marine Structures** 78: 103000. DOI: [10.1016/j.marstruc.2021.103000](https://doi.org/10.1016/j.marstruc.2021.103000).
- [9] F. Gao, Y. Shao, and W. Gho, (2007) "Stress and strain concentration factors of completely overlapped tubular joints under lap brace IPB load" **Journal of Constructional Steel Research** 63(3): 305–316. DOI: [10.1016/j.jcsr.2006.05.007](https://doi.org/10.1016/j.jcsr.2006.05.007).
- [10] D. S. Saini, D. Karmakar, and S. Ray-Chaudhuri, (2016) "A review of stress concentration factors in tubular and non-tubular joints for design of offshore installations" **Journal of Ocean Engineering and Science** 1(3): 186–202. DOI: [10.1016/j.joes.2016.06.006](https://doi.org/10.1016/j.joes.2016.06.006).
- [11] H. Nassiraei and P. Rezaeidoost, (2022) "Stress concentration factors in tubular T-joints reinforced with external ring under in-plane bending moment" **Ocean Engineering** 266: 112551. DOI: [10.1016/j.oceaneng.2022.112551](https://doi.org/10.1016/j.oceaneng.2022.112551).
- [12] A. Sadat Hosseini, M. R. Bahaari, and M. Lesani, (2020) "SCF distribution in FRP-strengthened tubular T-joints under brace axial loading" **Scientia Iranica** 27(3): 1113–1129. DOI: [10.24200/sci.2018.5471.1293](https://doi.org/10.24200/sci.2018.5471.1293).
- [13] T. C. Fung, C. Soh, T. Chan, and Erni, (2002) "Stress concentration factors of doubler plate reinforced tubular T joints" **Journal of Structural Engineering** 128(11): 1399–1412. DOI: [10.1061/\(ASCE\)0733-9445\(2002\)128:11\(1399\)](https://doi.org/10.1061/(ASCE)0733-9445(2002)128:11(1399)).
- [14] H. S. Mohamed, Y. Shao, C. Chen, and M. Shi, (2021) "Static strength of CFRP-strengthened tubular TT-joints containing initial local corrosion defect" **Ocean Engineering** 236: 109484. DOI: [10.1016/j.oceaneng.2021.109484](https://doi.org/10.1016/j.oceaneng.2021.109484).
- [15] S. Shojai, P. Schaumann, M. Braun, and S. Ehlers, (2022) "Influence of pitting corrosion on the fatigue strength of offshore steel structures based on 3D surface scans" **International Journal of Fatigue** 164: 107128. DOI: [10.1016/j.ijfatigue.2022.107128](https://doi.org/10.1016/j.ijfatigue.2022.107128).
- [16] A. Yosri, A. Zayed, S. Saad-Eldeen, and H. Leheta, (2021) "Influence of stress concentration on fatigue life of corroded specimens under uniaxial cyclic loading" **Alexandria Engineering Journal** 60(6): 5205–5216. DOI: [10.1016/j.aej.2021.04.004](https://doi.org/10.1016/j.aej.2021.04.004).
- [17] M. Jakubowski, (2015) "Influence of pitting corrosion on fatigue and corrosion fatigue of ship and offshore structures, part II: load-PIT-crack interaction" **Polish Maritime Research** 22(3): 57–66. DOI: [10.1515/pomr-2015-0057](https://doi.org/10.1515/pomr-2015-0057).
- [18] VSP. *White tiger field BK-1 in-air 2nd annual structural inspection report*. 2018.
- [19] VSP. *White tiger field MSP-6 in-air 3rd annual structural inspection report*. 2019.

- [20] A. Aidibi, S. Babamohammadi, N. Fatnuzzi, J. A. Correia, and L. Manuel, (2021) "Stress concentration factor evaluation of offshore tubular KT joints based on analytical and numerical solutions: Comparative study" **Practice Periodical on Structural Design and Construction** 26(4): 04021047. DOI: [10.1061/\(ASCE\)SC.1943-5576.000062](https://doi.org/10.1061/(ASCE)SC.1943-5576.000062).
- [21] M. Atteya, O. Mikkelsen, J. Wintle, and G. Ersdal, (2021) "Experimental and numerical study of the elastic SCF of tubular joints" **Materials** 14(15): 4220. DOI: [10.3390/ma14154220](https://doi.org/10.3390/ma14154220).
- [22] M. Lesani, A. S. Hosseini, and M. R. Bahaari. "Load bearing capacity of GFRP-strengthened tubular T-joints: Experimental and numerical study". In: *Structures*. 38. Elsevier. 2022, 1151–1164. DOI: [10.1016/j.istruc.2022.01.092](https://doi.org/10.1016/j.istruc.2022.01.092).
- [23] V. D. Chinh and H. T. T. Nguyễn, (2022) "Numerical models for stress analysis of non-uniform corroded tubular members under compression" **Structural Engineering and Mechanics** 84(4): 517. DOI: [10.12989/sem.2022.84.4.517](https://doi.org/10.12989/sem.2022.84.4.517).
- [24] H. S. Mohamed, Y. Shao, C. Chen, and M. Shi, (2021) "Static strength of CFRP-strengthened tubular TT-joints containing initial local corrosion defect" **Ocean Engineering** 236: 109484. DOI: [10.1016/j.oceaneng.2021.109484](https://doi.org/10.1016/j.oceaneng.2021.109484).
- [25] M. A. Sambo, G. R. Kol, and G. Betchewe, (2022) "Analysis of Stress Concentration Factors due to in-Plane Bending and out-of-Plane Bending Loads on Tubular TY-Joints of Offshore Structures" **Journal of Marine Science and Application** 21(4): 78–94. DOI: [10.1007/s11804-022-00303-9](https://doi.org/10.1007/s11804-022-00303-9).
- [26] ABS. *Guide for the fatigue assessment of offshore structures*. 2003.